A VRC H∞ design for dynamic thermal derating of induction machines

Author

Ali, SMN, Hossain, MJ, Hanif, A, Sharma, V, Kashif, M

Published

2018

Conference Title

2018 Australasian Universities Power Engineering Conference (AUPEC 2018)

DOI

10.1109/AUPEC.2018.8757950

A VRC H_∞ Design for Dynamic Thermal Derating of Induction Machines

S. M. Nawazish Ali*, Student member, IEEE, M. J. Hossain*, Senior member, IEEE, Athar Hanif†, Vivek Sharma*, Student member, IEEE and Muhammad Kashif*, Student member, IEEE
*School of Engineering, Macquarie University, NSW 2109, Australia
Email: syed-muhammad-nawazish.ali@hdr.mq.edu.au
†Department of Electrical Engineering, COMSATS Institute of Information Technology, Lahore, I.R. Pakistan

***Abstract*—Induction machines exhibit thermal derating in their performance during operation that causes sheer uncertainties in the controlling parameters such as stator and rotor resistances. It does not only affect the steady-state but also the dynamic response of an induction machine (IM). An output feedback variable resistance controller (VRC), which is inherently an H_∞ linear parameter varying (LPV) controller, is proposed to compensate this thermal derating caused by stator resistance variations. An L_2 gain bound and internal stability are ensured by linear matrix inequalities (LMIs). IM speed control is established by using input/output feedback linearization (I/O-FL). The proposed controller is implemented for a 30 kW induction motor in MATLAB®Simulink environment. Nonlinear simulation results show excellent performance tracking for the thermally derated dynamic IM characteristics in the presence of varying stator resistance and an applied load torque.**

***Index Terms*—Induction machine; Dynamic thermal deration; Stator resistance variation; VRC design; Linear Matrix Inequalities**

I. Introduction

Induction machines show a promising performance in the industrial as well as automotive sector. This is mainly due to greater initial torque, reduced cost, consistency in wide range speed operation, relatively high power density, inherent de-excitation against inverter faults and, little maintenance [1]. The robust operation of an IM significantly depends on its electromechanical and thermal core properties [2]. IMs suffer from parameter (stator and rotor resistance) uncertainties during operation due to loading, hot/cold environments etc. High power IMs experience even 115°C temperatures during their operation [3]. Moreover, the dynamic characteristics of an IM also change with temperature variations. These variations in machine terminal parameters such as speed, torque and flux are of high importance in industrial as well as automotive sector applications [4].

Stator resistance variation is a significant problem and causes unstable IM drive operation [5]. The life expectancy of stator insulation is halved with a temperature rise of even 10°C, once its thermal limit is reached [6]. IM losses enhance temperature variations that cause changes in stator resistance and ultimately lead to higher copper loss, worsening the IM flux [7]. Even the $d-q$ rotor flux linkages vary with the stator resistance [8]. Stator resistance variations at light loads cause significantly higher IM iron losses than does the airgap power. The uncertainities in stator resistance cause poor performance of field oriented control (FOC) for IMs [9]. This issue is addressed by the proposed VRC acting as a robust LPV controller, along with linear matrix inequalities (LMIs) synthesis using H_∞ control. LPV control technique provides better gain scheduling and robustness, keeping the actual plant dynamics intact [10]. With limited uncertainties in IM parameters, an LPV control has been presented in [11]. By using a Quasi LPV strategy, an IM control has been developed in [12]. For controlling the shaft angle of an IM, an LPV control design has been discussed in [13], but motor resistance variations are not considered. LPV observer has been proposed in [14] for an IM nonlinear model. The context is focused on flux estimation. The rotor current frequency and IM speed have been controlled by an LPV technique in [15]. The authors have developed and presented the steady state and LPV controlled dynamic characteristics of an IM against rotor resistance variations in [16]–[18].

This paper presents the nonlinear dynamic behavior of an IM against stator resistance variations and also proposes a robust novel LPV controller using linear matrix inequalities (LMIs) approach to cater for the stator resistance variations for dynamic thermal derating in an IM in the form of a VRC. The control technique is validated for the speed, torque and flux tracking of a 30 kW induction machine. The remaining paper is organized as follows: Section II presents the IM mathematical modeling. Section III discusses the VRC control design for the IM dynamic behavior and I/O-FL for the speed and flux control. Section IV gives the simulation results and analysis. Section V gives a conclusion and proposed future work.

II. IM Nonlinear Dynamic Model

A $d-q$ axis stationary-frame IM model has been extracted from [19].

$$\begin{aligned}
\dot{\omega}_R &= \lambda_0(\psi_{dr}i_{qs} - \psi_{qr}i_{ds}) - (\lambda_7 B\omega_R) - (\lambda_7\tau_L)\\
\dot{i}_{ds} &= -\lambda_1 i_{ds} + \lambda_2\psi_{dr} + \lambda_3\psi_{qr} + \lambda_4 V_{ds}^2\\
\dot{i}_{qs} &= -\lambda_1 i_{qs} + \lambda_2\psi_{qr} - \lambda_3\psi_{dr} + \lambda_4 V_{qs}^2\\
\dot{\psi}_{dr} &= -\lambda_5\psi_{dr} - n_P\omega_R\psi_{qr} + \lambda_6 i_{ds}\\
\dot{\psi}_{qr} &= -\lambda_5\psi_{qr} + n_P\omega_R\psi_{dr} + \lambda_6 i_{qs} \qquad (1)
\end{aligned}$$

TABLE I
IM PARAMETERS

Parameter	Description	Value
n_P	number of pole-pairs	2
L_s	stator self-inductance	0.0425 H
L_r	rotor self-inductance	0.043 H
R_s	stator resistance	0.22 Ω
R_r	rotor resistance	0.209 Ω
L_m	magnetizing inductance	0.04 H
J	moment of inertia	0.124 kg.m^2
B	damping coefficient	0.01 N.m.sec.rad^{-1}

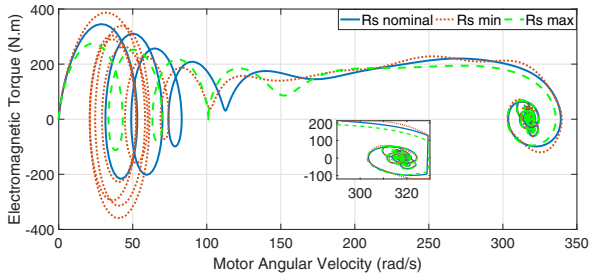

Fig. 1. Dynamic τ_E-ω_R response for varying stator resistance

where λ_0=$\frac{n_P L_m}{J L_r}$, λ_1=$\frac{(L_m^2 R_r + L_r^2 R_s)}{\sigma L_s L_r^2}$, λ_2=$\frac{L_m R_r}{\sigma L_s L_r^2}$, λ_3=$n_P \frac{L_m \omega_R}{\sigma L_s L_r}$, λ_4=$\frac{1}{\sigma L_s}$, $\sigma = 1 - \frac{L_m^2}{L_s L_r}$, λ_5=$\frac{R_r}{L_r}$, λ_6=$\frac{L_m R_r}{L_r}$, λ_7=$\frac{1}{J}$. i_{ds} and i_{qs} are the $d-q$ stator currents, ψ_{dr} and ψ_{qr} are the $d-q$ rotor fluxes, V_{ds} and V_{qs} are the stator voltages and ω_R represents the motor angular velocity. The IM parameters are given in Table I.

The IM electromagnetic torque is given as:

$$\tau_E = \frac{3}{2} n_P \lambda_0 (\psi_{dr} i_{qs} - \psi_{qr} i_{ds}) \tag{2}$$

A. IM Dynamic Thermal Derating in Industrial/Traction Application

The nonlinear dynamic model of a 3-ϕ IM has been simulated in MATLAB®Simulink for different values of stator resistance (R_s) caused by varying temperature. The response is expressed in Fig. 1. Table II gives the values of stator resistance.

As shown in the figure, an IM used in industrial/traction application will never be able to provide the desired torque and speed due to varying R_s during its operation that will ultimately reduces its performance efficiency. The zoomed graph represents the trajectories with varying applied load torque τ_L and its steady state points.

TABLE II
VALUES OF STATOR RESISTANCE

Stator Resistance (R_s)	Value
$R_{s\,max}$	0.44 Ω
$R_{s\,nominal}$	0.22 Ω
$R_{s\,min}$	0.11 Ω

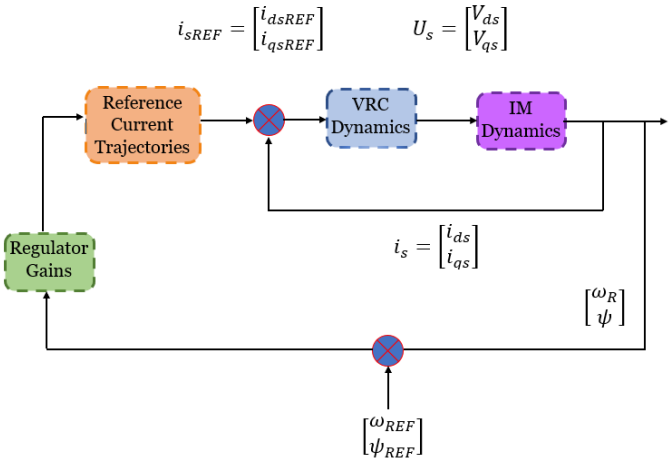

Fig. 2. Feedback control system architecture

III. VRC DESIGN

To cater for the thermal issues described in the previous section, a VRC (inherently an LPV controller) has been designed for the dynamic τ_E-ω_R nonlinear response over the entire stator resistance range [$R_{s\,min}$ $R_{s\,max}$].

A. Control System Architecture

The control system architecture for the closed-loop structure is shown in Fig. 2. It comprises two major sections:

1) $d-q$ stator currents control: A VRC is designed for the $d-q$ stator currents closed loop. It is scheduled with the stator resistance R_s and is represented as:

$$G(\Theta(t)) : \dot{x} = A(\Theta(t))x + Bu$$
$$y = Cx + Du \tag{3}$$

where $\Theta(t)$=$R_s(t)$ is a varying parameter with respect to time. The VRC system matrix is given as:

$$A(\Theta(t)) = \begin{bmatrix} -(\frac{\Theta}{\sigma\xi Lr^2} + \frac{1}{\sigma\chi_s}) & 0 & \frac{\delta\Theta}{\sigma L_s L_r} & 0 \\ 0 & -(\frac{\Theta}{\sigma\xi Lr^2} + \frac{1}{\sigma\chi_s}) & 0 & \frac{\delta\Theta}{\sigma L_s L_r} \\ \delta\Theta & 0 & \frac{\Theta}{L_r} & 0 \\ 0 & \delta\Theta & 0 & \frac{\Theta}{L_r} \end{bmatrix} \tag{4}$$

$$B = \begin{bmatrix} \frac{1}{\gamma} & 0 \\ 0 & \frac{1}{\gamma} \\ 0 & 0 \\ 0 & 0 \end{bmatrix} C = \begin{bmatrix} 1 & 0 & 0 & 0 \\ 0 & 1 & 0 & 0 \end{bmatrix} D = \begin{bmatrix} 0 & 0 \\ 0 & 0 \end{bmatrix} \tag{5}$$

where $\xi = L_s/L_m^2$, $\chi_s = L_s/R_s$, $\delta = L_m/L_r$, $\gamma = \sigma L_s$. B, C, D are fixed matrices. The input, output and state vectors are:

$$u(t) = [V_{ds}\ V_{qs}]^T; y(t) = [i_{ds}\ i_{qs}]^T; x(t) = [i_{ds}\ i_{qs}\ \psi_{dr}\ \psi_{qr}]^T \tag{6}$$

The state-space representation of a generalized VRC plant is given by:

$$\begin{aligned} \dot{x}(t) &= A(\Theta(t))x(t) + B_w(\Theta(t))w(t) + B_u(\Theta(t))u(t) \\ z(t) &= C_z(\Theta(t))x(t) + D_{zw}(\Theta(t))w(t) + D_{zu}(\Theta(t))u(t) \\ v(t) &= C_v(\Theta(t))x(t) + D_{vw}(\Theta(t))w(t) \end{aligned} \tag{7}$$

where $w(t)$=$[i_{dsref}\quad i_{qsref}]^T$; $v(t)$=$[i_{ds}\quad i_{qs}]^T$; $u(t)$=$[V_{ds}\ V_{qs}]^T$.

The state-space representation of the VRC gain schedule output feedback controller is:

$$\begin{aligned} \dot{x}_K &= A_K(\Theta)x_K + B_K(\Theta)y \\ u &= C_K(\Theta)x_K + D_K(\Theta)y \end{aligned} \tag{8}$$

The following LMIs are implemented to ensure L_2 gain bound and internal stability [20]:

$$\begin{bmatrix} AY + YA^T + B_u\tilde{C}_K + (B_u\tilde{C}_K)^T & \tilde{A}_K + A + \\ * & A^TX + XA + \\ * & * \\ * & * \\ B_u\tilde{D}C_v & B_w + B_u\tilde{D}D_{vw} \\ \tilde{B}_KC_v + (\tilde{B}_KC_v)^T & XB_w + \tilde{B}_KD_{vw} \\ & -\gamma I \\ & * \end{bmatrix} \begin{bmatrix} (C_zY + D_{zu}\tilde{C}_K)^T \\ (C_z + D_{zu}\tilde{D}_KC_v)_T \\ (D_{zw} + D_{zu}\tilde{D}D_{vw})^T \\ -\gamma I \end{bmatrix} < 0 \tag{9}$$

$$\begin{bmatrix} Y & I \\ I & X \end{bmatrix} > 0 \tag{10}$$

(*) represents symmetry. The first LMI has the objective to minimize γ, whereas the second is for the symmetric positive definite condition. The optimized value of γ is 0.8020. The controller gains A_K, B_K, C_K and D_K can be calculated by using the following equations:

$$\begin{aligned} A_K = N^{-1}(\tilde{A}_K - NB_KC_vY - XB_uC_KM^T - \\ X(A + B_uD_KC_v)Y)(N^T)^{-1} \end{aligned} \tag{11}$$

$$B_K = N^{-1}(\tilde{B}_K - XB_uD_K) \tag{12}$$

$$C_K = (\tilde{C}_K - D_KC_vY)(M^T)^{-1} \tag{13}$$

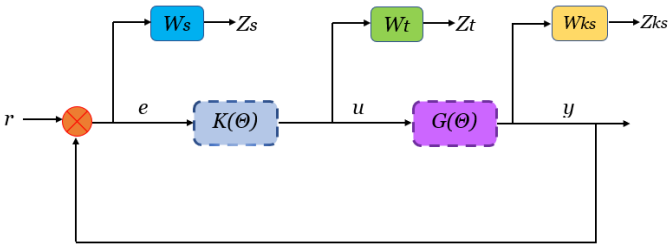

Fig. 3. H_∞ sensitivity gains structure

$$D_K = \tilde{D}_K \tag{14}$$

where N and M are the matrices such that

$$I - XY = NM^T \tag{15}$$

The matrix $A(\Theta(t))$ in (4) is given by:

$$A(\Theta(t)) = A(R_s) = A_0 + \Theta_1A_1 = A_0 + (R_s)A_1 \tag{16}$$

The convex decomposition of $\Theta(t)$ is given as:

$$\Theta(t) = \alpha_1\Theta_1 + \alpha_2\Theta_2 \tag{17}$$

with

$$\sum_{i=1}^{2} \alpha_i = 1\ and\ \alpha \geq 0$$

where α_i gives the polytopic parameter range corner. The corner values of the parameter range are as follows:

$$\Theta_{11} = (0, R_{s\,min}), \Theta_{12} = (0, R_{s\,max}) \tag{18}$$

The plant matrix corresponding to the vertices of Θ is given by:

$$G(\Theta) = \alpha_1G(\Theta_{11}) + \alpha_2G(\Theta_{12}) \tag{19}$$

$$\alpha_1 = \frac{R_s(t) - R_{s\,min}}{R_{s\,max} - R_{s\,min}}; \alpha_2 = \frac{R_s(t) - R_{s\,max}}{R_{s\,max} - R_{s\,min}} \tag{20}$$

The VRC structure is given by polytopic representation as:

$$K(\Theta) = \sum_{i=1}^{2} \alpha_i \begin{bmatrix} A_K(\Theta_i) & B_K(\Theta_i) \\ C_K(\Theta_i) & D_K(\Theta_i) \end{bmatrix} \tag{21}$$

The desired performance objectives of the IM control system can be achieved by using the weighting gains W_s, W_t and W_{ks} as shown in Fig. 3. Their values and functions are given in Table III. The actual output vector $z = [z_s\ z_t\ z_{ks}]^T$ in (7) can be derived from this figure.

TABLE III
WEIGHTING GAIN VALUES

Weighting Gain	Value
W_t (complementary sensitivity)	$\frac{(0)s+w_T}{(0)s+1}$ where w_T=0.8
W_s (sensitivity)	$\frac{(1/M_s)s+w_B}{s+w_B A}$ where w_B=bandwidth=550 M_s=sensitivity upper bound=2.0 A=factor for attenuation=1/500
W_{ks} (control sensitivity)	1/200

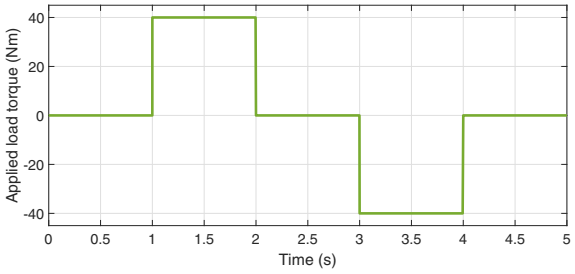

Fig. 4. An applied bi-polar load torque

2) Rotor speed & IM flux control: The $d-q$ stator reference currents with respect to motor speed and flux are generated by the input/output feedback linearization (I/O-FL). An augmented plant scheme is often used in LPV control structure for an appropriate design specifications. A regulator with proper gain values is designed to achieve tracking by classic control techniques. The $d-q$ stator reference currents are:

$$i_{dsREF} = \frac{\psi_{dr}}{\lambda_6}(\frac{\dot{\psi}}{\psi}+\lambda_5)+\frac{\psi_{qr}}{n_P\lambda_0\lambda_7\psi^2}(-\dot{\omega}_R-\lambda_7\tau_L-\lambda_7 B\omega_R) \tag{22}$$

$$i_{qsREF} = \frac{\psi_{qr}}{\lambda_6}(\frac{\dot{\psi}}{\psi}+\lambda_5)+\frac{\psi_{dr}}{n_P\lambda_0\lambda_7\psi^2}(\dot{\omega}_R+\lambda_7\tau_L+\lambda_7 B\omega_R) \tag{23}$$

where the rotor speed derivative ($\dot{\omega}_R$) is given in (1) and the motor flux derivative ($\dot{\psi}$) is given by:

$$-\lambda_5\psi+\lambda_6\frac{\psi_{dr}i_{ds}+\psi_{qr}i_{qs}}{\psi} \tag{24}$$

IV. VRC PERFORMANCE VALIDATION

The VRC-IM feedback control system of Fig. 2 is implemented in MATLAB®Simulink with an applied load torque in the form of a square wave that includes the motoring as well as the generating operation of the IM as shown in Fig. 4 . The varying stator resistance is given in the form of a square wave encompassing the entire operating range i.e. $[0.5R_s\ 2R_s]$ as shown in Fig. 5.

A. $d-q$ axis Stator Currents

The performance tracking of the $d-q$ axis stator currents is shown in Fig. 6 and Fig. 7 respectively. It clearly concludes that the output stator currents perfectly follow the reference

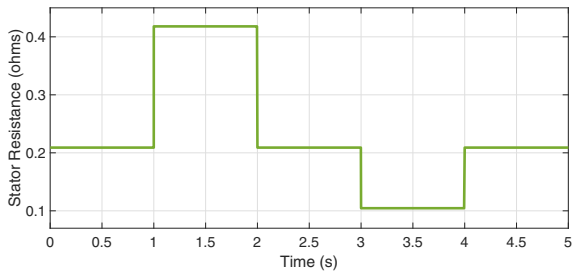

Fig. 5. Varying stator resistance

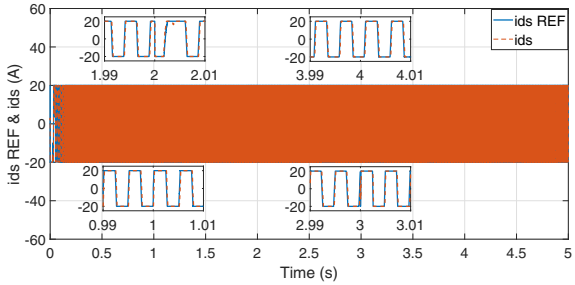

Fig. 6. Tracking of $d-axis$ stator current

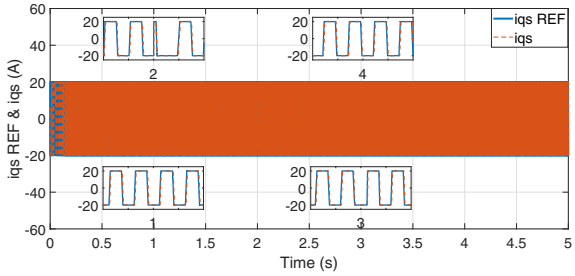

Fig. 7. Tracking of $q-axis$ stator current

currents extracted by I/O-FL, validating the robustness of the proposed control architecture. Moreover, further analysis of these results highlights the varying stator resistance and an applied bi-polar load torque effects in the zoomed sections of the plot. These currents are bounded by saturation limits $\leq 20A$. Hence, the thermal derating causes stator currents degradation resulting in low IM efficiency and increased energy consumption.

B. $d-q$ axis Stator Voltages

The control effort for the VRC is provided in the form of $d-q$ axis stator voltages as shown in Fig. 8. The control voltage signals are bounded by saturation limits $\leq 380V$. A conclusion can be drawn from the zoomed plots of this result that the control signals are also affected by the varying stator resistance caused by the change in IM temperature and an applied load torque, although the robust VRC maintains the tracking of reference signals by providing the necessary control effort.

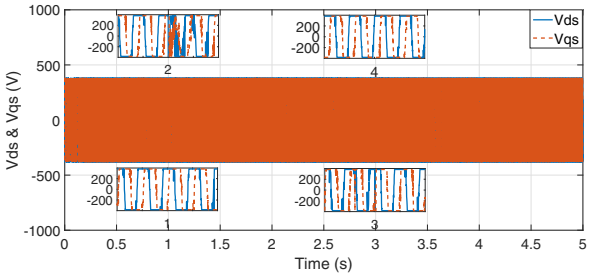

Fig. 8. Control effort as $d-q$ axis stator voltages

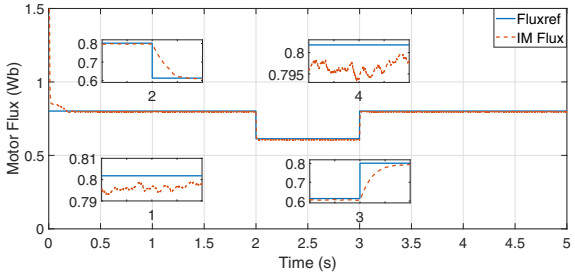

Fig. 9. Motor flux

C. IM Flux

IM flux has a significant role in machine applications (industrial/automotive) as it derives the IM electromagnetic torque. It is given in Fig. 9. The flux tracking validates the efficacy and robustness of the designed VRC as well as I/O-FL technique. Further analysis of the zoomed plots depicts the flux variations caused by the varying stator resistance due to changes in IM temperature and an applied load torque. Even a slight flux instability causes a significant variation in machine torque.

D. Dynamic τ_E-ω_R Controlled Response

The dynamic thermal derating in the IM torque-speed response controlled by VRC against an applied load torque and varying stator resistance due to changes in IM temperature is shown in Fig. 10. As discussed in previous results, the variation in the $d-q$ axis stator currents and IM flux varies the electromagnetic torque demand given in (2). Ultimately, the IM efficiency as well as its energy consumption will also be affected. The performance tracking validates the robust design of the VRC as well as the reference currents extraction by I/O-FL.

V. A $3-\phi$ IM CASE STUDY

A $3-\phi$ wound type 4-pole induction motor with a rated voltage of 460 V is given in [21]. Its impedance parameters are given in Table IV. The torque-speed curve for this steady-state motor model has been plotted against the varying stator resistance which clearly shows the influence of resistance variation due to temperature change over the performance of induction motor. The variation in stator resistance is considered in the

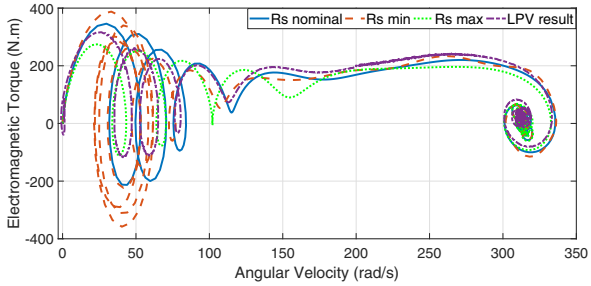

Fig. 10. Dynamic τ_E-ω_R controlled response for varying stator resistance

TABLE IV
IMPEDANCE PARAMETERS

Parameter	Value
R_s	0.641 Ω
R_r	0.332 Ω
X_s	1.106 Ω
X_r	0.464 Ω
X_m	26.3 Ω

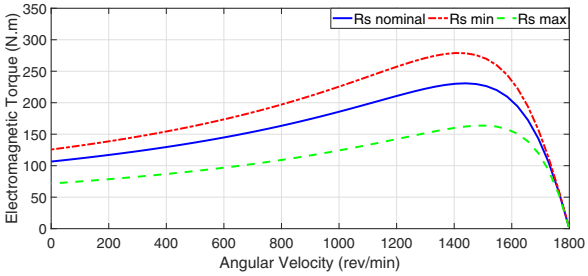

Fig. 11. Effect of stator resistance variation on IM performance

range $[0.5R_s\ 2R_s]$. It is shown in Fig. 11. The formulae used to develop the mentioned characteristics are given in (25)-(29).

IM Thevinin voltage is given by:

$$V_{th} = V_\phi \times \frac{X_m}{\sqrt{R_s^2 + (X_s + X_m)^2}} \tag{25}$$

IM Thevinin resistance is given by:

$$R_{th} \approx R_s \times \frac{X_m}{\sqrt{R_s^2 + (X_s + X_m)^2}} \tag{26}$$

IM Thevinin reactance is given by:

$$X_{th} \approx X_s \tag{27}$$

IM mechanical speed is given by:

$$n_M = (1-s)n_{sync} \tag{28}$$

IM maximum torque is given by:

$$\tau_{MAX} = \frac{3 \times V_{th}^2}{2 \times [R_{th} + \sqrt{R_{th}^2 + (X_{th} + X_r)^2}]} \tag{29}$$

VI. Conclusion

In this paper, an output feedback VRC is presented for the varying stator resistance of an induction machine during its operation in the presence of an applied load torque. Linear matrix inequalities and H_∞ sensitivity gains are used to ensure the internal stability of the designed control system. Simulation results including the nonlinear dynamic thermal derating of induction machine torque-speed behaviour are presented to validate the controller efficacy. It is found that the VRC controlled dynamic behavior of IM is quite close to the dynamic behaviour for nominal stator resistance. A case study discussing the stator resistance effects on the steady state IM model is also presented with mathematical calculations. In future, the results will be validated on a proper hardware test bench to ensure the robustness of the proposed controller in a practical scenerio.

Acknowledgment

The authors are grateful to the School of Engineering, Macquarie University, Sydney, Australia and the Center for Automotive Research (CAR), The Ohio State University, Columbus, U.S.A. for providing research direction.

References

[1] A. Hanif, A. I. Bhatti, and Q. Ahmed, "Managing thermally derated torque of an electrified powertrain through lpv control," *IEEE/ASME Transactions on Mechatronics*, vol. 23, no. 1, pp. 364–376, 2018.

[2] G. Bramerdorfer, A. Cavagnino, and S. Vaschetto, "Importance of thermal modeling for design optimization scenarios of induction motors," in *Energy Conversion Congress and Exposition (ECCE), 2017 IEEE*. IEEE, 2017, pp. 4666–4672.

[3] J. T. M. Valenzuela and J. Rooks, "Thermal evaluation of tefc induction motors operating on frequency-controlled variable-speed drives," *IEEE Transactions on Industry Applications*, vol. 40, no. 2, pp. 692–698, 2004.

[4] P. Gnacinski, "Derating of an induction machine under voltage unbalance combined with over or undervoltages," *Energy Conversion and Management*, vol. 50, no. 4, pp. 1101–1107, 2009.

[5] M. S. Zaky and M. K. Metwaly, "Sensorless torque/speed control of induction motor drives at zero and low frequencies with stator and rotor resistance estimations," *IEEE Journal of Emerging and Selected Topics in Power Electronics*, vol. 4, no. 4, pp. 1416–1429, 2016.

[6] W. Pawlus, J. T. Birkeland, H. Van Khang, and M. R. Hansen, "Identification and experimental validation of an induction motor thermal model for improved drivetrain design," *IEEE Transactions on Industry Applications*, vol. 53, no. 5, pp. 4288–4297, 2017.

[7] J. Holtz and J. Quan, "Sensorless vector control of induction motors at very low speed using a nonlinear inverter model and parameter identification," *IEEE Transactions on Industry Applications*, vol. 38, no. 4, pp. 1087–1095, 2002.

[8] B. Karanayil, M. F. Rahman, and C. Grantham, "Online stator and rotor resistance estimation scheme using artificial neural networks for vector controlled speed sensorless induction motor drive," *IEEE Transactions on Industrial Electronics*, vol. 54, no. 1, pp. 167–176, 2007.

[9] E. D. Mitronikas, A. N. Safacas, and E. C. Tatakis, "A new stator resistance tuning method for stator-flux-oriented vector-controlled induction motor drive," *IEEE Transactions on Industrial Electronics*, vol. 48, no. 6, pp. 1148–1157, 2001.

[10] K. Zhou, J. C. Doyle, K. Glover *et al.*, *Robust and optimal control*. Prentice Hall New Jersey, 1996, vol. 40.

[11] K. Dalila, M. Abdessalem, D. Said, and L. Chrifi-Alaoui, "Robust linear parameter varying induction motor control with polytopic models," *Serbian Journal of Electrical Engineering*, vol. 10, no. 2, pp. 335–348, 2013.

[12] F. Farhani, C. B. Regaya, A. Zaafouri, and A. Chaari, "A quasi linear parameter varying approach to robust control of an induction machine," in *Systems, Signals & Devices (SSD), 2013 10th International Multi-Conference on*. IEEE, 2013, pp. 1–5.

[13] F. Blanchini, D. Casagrande, S. Miani, and U. Viaro, "An lpv control scheme for induction motors," in *Decision and Control (CDC), 2012 IEEE 51st Annual Conference on*. IEEE, 2012, pp. 7602–7607.

[14] A. Hanif, A. Bhatti, and Q. Ahmed, "Estimation of thermally de-rated torque of an hev drive using robust lpv observer," in *American Control Conference (ACC), 2016*. IEEE, 2016, pp. 1530–1535.

[15] D. K. Abdessalem, D. Said *et al.*, "Linear parameter varying induction motor control with two-degree-of freedom controller," in *Power Engineering, Energy and Electrical Drives (POWERENG), 2013 Fourth International Conference on*. IEEE, 2013, pp. 1748–1752.

[16] S. N. Ali, A. Hanif, and Q. Ahmed, "Review in thermal effects on the performance of electric motors," in *Intelligent Systems Engineering (ICISE), 2016 International Conference on*. IEEE, 2016, pp. 83–88.

[17] A. Hanif, S. N. Ali, Q. Ahmed, A. Bhatti, G. Yin, and M. H. Jaffery, "Effect of variation in rotor resistance on the dynamic performance of induction motor," in *Control Conference (CCC), 2016 35th Chinese*. IEEE, 2016, pp. 9524–9529.

[18] S. N. Ali, A. Hanif, M. J. Hossain, and V. Sharma, "An lpv h∞ control design for the varying rotor resistance effects on the dynamic performance of induction motors," in *Industrial Electronics (ISIE), 2018 27th International Symposium on*. IEEE, 2018, pp. 114–119.

[19] R. Marino, S. Scalzi, P. Tomei, and C. Verrelli, "Fault-tolerant cruise control of electric vehicles with induction motors," *Control Engineering Practice*, vol. 21, no. 6, pp. 860–869, 2013.

[20] H. Werner, "Optimal and robust control-lecture notes," *Technical University Hamburg-Harburg, Institute of Control Engineering*, 2004.

[21] S. Chapman, *Electric machinery fundamentals*. Tata McGraw-Hill Education, 2005.